npj Computational Materials

https://doi.org/10.1038/s41524-026-02144-4

Article in Press

Linear bond strength-bond order relationship in covalent interactions

Received: 17 January 2026

Accepted: 11 May 2026

Cite this article as: Zhao, S., Ni, Y., Peng, Q. *et al.* Linear bond strength-bond order relationship in covalent interactions. *npj Comput Mater* (2026). https://doi.org/10.1038/s41524-026-02144-4

Shuai Zhao, Yong Ni, Qing Peng & Yujie Wei

Linear bond strength-bond order relationship in covalent interactions

Shuai Zhao[1,2], *Yong Ni*[1], *Qing Peng*[3], & *Yujie Wei*[2,*]

[1]Department of Modern Mechanics, University of Science and Technology of China, Hefei, Anhui, 230026, China

[2] Mechano-X Institute, Applied Mechanics Laboratory, Department of Engineering Mechanics, Tsinghua University, Beijing, 100084, China

[3] School of Power and Mechanical Engineering, Wuhan University, Wuhan, 430072, China.

Corresponding Author

*yujie_wei@tsinghua.edu.cn (Yujie Wei)

Abstract: Covalent bonding between atoms (molecules) constitutes the rich diversity of nature ranging from the very recently realized one-electron carbon-carbon σ-bond to the well-known hybridized bonds in diamond. This diversity in covalent interactions raises fundamental questions about universal correlations between their electronic structure and mechanical properties. We unveil in this report a general linear correlation of bond strength with the bond order of C–C covalence. From the one-electron σ-bond predicted by Pauling [1] and vindicated by Shimajiri et al. [2] with a bond strength of 1.49 nN and a bond length of 1.98 Å, all the way to the six-electron σ + 2π bond of 25.72 nN in bond strength 1.20 Å in length, the strength and the order of C–C bonds follow a linear relationship with a slope of 8.9 nN/order. The linearity persists in 13 types of covalent interactions, with prominent examples including Si–Si and B–N covalent bonds. Such a linear scaling law establishes a broad guidance for predictive tuning of covalent bond strengths via bond order engineering.

Keywords: covalent carbon bond, bond order, bond strength, one-electron σ-bond

Introduction

Covalent bonding as a fundamental building block of organic and inorganic materials exhibits a rich hierarchy of bonding configurations governed by electron occupancy and orbital hybridization. Taking the well-explored carbon as a model case, covalent carbon-carbon (C–C) bonds are classified into four categories based on their bonding orbitals and electron delocalization, including single (σ), double (σ + π), triple (σ + 2π), and delocalized π bonds in aromatic systems[1, 3]. A σ-bond is formed by head-on overlap of hybrid orbitals, while π bonds have lateral orbital overlaps, shortened bond length and enhanced bond strength[4-7]. From σ-bond in diamond to delocalized π bonds in graphene, its versatility underpins carbon's unparalleled role in materials science[8-10]. While conventional bonding configurations have been extensively studied with well-established structure-property relationships, odd-electron bonds remain enigmatic despite their potential to unlock unprecedented material functionalities[11-14]. Historically, odd-electron bonds are regarded as transient intermediates in radical reactions and are weaker than even-electron bonds, as postulated by Pauling in 1931[15-18]. A recent breakthrough provides direct evidence on the existence of a carbon-carbon one-electron σ-bond (C···C)[2]. Those authors realized a stable molecular cation of hexaphenylethane **1**, which is termed as $\mathbf{1}^{\cdot+}$ and has an elongated C···C bond of 2.921 Å in length. This bond, stabilized by a single electron, broadens the mechanical and electronic diversity of C–C bonding family which lies at the heart of material innovation[3, 19].

The versatile C–C bonds raise as a corollary the interest in their mechanical dependence on bond order[20]. Furthermore, while the existence of one-electron σ-bond predicted by Pauling in 1931[15-17] has been demonstrated by Shimajiri et al.[2], one may wonder whether there are common features among other types of covalence with a variety of bond orders. We aim to explore the two points in this report. We pick C–C covalence to decode the mechanical properties of bonds of distinct bond orders through first-principles calculations. A systematical investigation on 13 covalent systems across 7 elements (B, C, N, O, Si, P and S) is performed. Those systems include most quasi-diatomic bonds with multiple bond orders[21]. This exploration unveils a linear relationship between the bond strength and bond order in those covalent systems.

Results and Discussion

A. One-electron σ-bond in cation $\mathbf{1}^{\cdot+}$

Being a prominent example of the one-electron σ-bond, we zoom in on the molecular structure of the cation $\mathbf{1}^{\cdot+}$ in Fig. 1(a). Using natural bond orbital (NBO) analysis, we explore the destabilizing electronic features in this one-electron bond system. The occupancy of bonding orbital between C···C is 0.768, and its antibonding orbital has an occupancy of 0.345. We hence obtain a bond order of 0.216 for cation $\mathbf{1}^{\cdot+}$. In contrast, a typical two-electron σ bond has a bond order of ~1.0[22]. The NBO energy of the C···C bond of cation $\mathbf{1}^{\cdot+}$ is -8.76 eV, in contrast, a typical alkane C–C bond has an NBO energy of -22.77 eV[23]. We further perform EDA of the two vdW planes consisting of two proximal aryl fragments (Fig. S1, Supporting Information). The sobEDA method [24] breakdowns the interaction energies into six parts, namely the electrostatic interaction, exchange repulsion, Pauli repulsion, orbital interaction, density functional theory (DFT) correlation and dispersion correlation. Their respective contributions are 206.9, -76.4, 228.6, -39.1, -36.7, and -101.1 kJ/mol, in turn. In combination, the net inter-fragment repulsion energy is 152.2 kJ/mol. The positive Pauli repulsion and total repulsion between the vdW planes are balanced by the attraction of C–C bond at the bottom part in Fig. S1(a). During the potential energy scanning, the vdW planes are replaced with hydrogen atoms in the truncated model (Fig. S1(b)) to preserve the coordination environment while allowing for separation in the one-electron bond. All other degrees of freedom are fully relaxed. We show in Fig. S1(c) the change of potential energy during the bond separation, from which we see an energy barrier up to 1008.3 kJ/mol for bond dissociation. The barrier far exceeds those repulsive energies mentioned above, and demonstrates its stability.

The energy stretching curve (Fig. 1(b)) is influenced not only by the one-electron σ-bond interaction but also by the interplay of vdW forces and covalent bonds within the base plane, as seen from the dashed lines from the counterpart of an isolated σ-bond ($H_3C\cdots CH_3^+$). We show with the methane cation ($H_3C\cdots CH_3^+$) distinct electronic signatures of the carbon-carbon one-electron σ-bond (Fig. S2, Supporting Information). The α-spin orbital occupation number between the two carbon atoms is 1, while that of β-spin orbital occupation is ~0, consistent with a formal single-electron bonding interaction. As a comparison, carbon-hydrogen covalence exhibits conventional two-electron bonding characteristics, evidenced by their double spin orbitals ($\alpha\sim1, \beta\sim1$). The non-bonded C-H interactions exhibit an exceptionally weak second-order perturbation energy E(2) of 0.25 kcal/mol, well below the empirically established threshold of 0.5 kcal/mol for significant intermolecular interactions[22]. This justifies their negligible contribution to the system's electronic structure. Similarly, non-bonded hydrogen-hydrogen interactions demonstrate no meaningful E(2) values, suggesting the absence of direct H···H orbital coupling. This conclusion is further supported by the complete lack of spatial overlap between σ(C1-H) and σ(C2-H) orbitals in the supplementary Fig. S2(a) – a critical observation given hydrogen's lack of lone pairs, which restricts potential interactions to σ-orbital pathways. Topological analysis of the electron density (Fig. S2(b)) provides additional confirmation: No bond critical points (BCPs)[25] are observed between non-bonded C···H or H···H pairs. Absence of BCPs definitively rules out hydrogen bond formation or other non-covalent interactions that might complicate our mechanical property calculations[26, 27]. The collective evidence establishes that the simplified model successfully isolates the C-C one-electron σ-bond, ensuring subsequent mechanical analyses specifically probe this unique interaction without interference intermolecular forces, at least at a negligible level.

After each increment of distance between a C–C bond subjected to stretching, we relax the rest atoms in the molecule. The external force is defined as the negative derivative of the potential energy with respect

to the bond separation. In convention, we refer the bond to be in tension when the force is positive and negative forces correspond to its compressive state. The distinction in the force-separation curve of the isolated $H_3C\cdots CH_3^+$ system and that of cation $\mathbf{1}^{\cdot+}$ demonstrates how these ancillary interactions modulate the mechanical response relative to the idealized single-bond scenario. To explicitly decompose the force exclusively acting on the one-electron σ-bond in this system, we conduct EDA method to compute the intrinsic C···C interaction energy at various C···C bond separation. The resulting force profile (Fig. 1(c)) reveals that the bond within the molecular cation $\mathbf{1}^{\cdot+}$ is perceivably lower relative to the isolated one-electron bond system, potentially due to electronic delocalization. At its equilibrium configuration, the SOMO of cation $\mathbf{1}^{\cdot+}$ exhibits delocalization over the entire aryl groups, with partial bonding between the two carbon atoms of one-electron bond (Fig. 1(d, 3)). The electron density distribution of the C···C bond exhibits a peanut-shaped SOMO. The bond stiffness is 57.5 N/m, in line with the frequency-based estimates, confirming the internal consistency of our mechanical analysis. A transition from the rugby-ball shaped electron density distribution (Fig. 1(d, 1-2)) to the peanut-shaped profile (Fig. 1(d, 3)) marks the outset of strain softening when gradually separating the C···C bond apart [28]. Further separation leads to a SOMO showing a nodal plane with a wave function of zero amplitude (Fig. 1(d, 4)), which is the starting point of homolytic cleavage of covalent bonds[29]. Note non-covalent forces beyond this point remain active through collective electronic effects[30]. At a separated distance r = 3.62 Å when the bond is stretched by 0.77 Å (Fig. 1(d, 5)), the overlapped electron density distribution of the C···C bond disappears.

B. Isolated carbon-carbon odd-electron bonds

To establish a fundamental understanding of the diatomic bonds, we start with the simplified systems with odd-electron C–C bonds composed of two carbon atoms, as depicted in Fig. 2(a). Isolating the C···C one-electron σ-bond enables us to probe its unique interaction free from interference from ancillary intermolecular forces. This approach is in parallel with the study of ethane[31-35], ethylene[36-39], and ethyne cations[40, 41] with varying bond orders.

At equilibrium, the C–C odd-electron bonds have perceivably longer interactions in contrast to even-electron bonds, with the ethane cation being the longest. Fig. 2(b) illustrates the Kohn-Sham orbitals of the SOMO of each cation[42], and that of the ethane cation is characterized by one σ-orbital—indicative of a one-electron σ-bond, whereas the ethylene and ethyne cations are characterized by π-orbitals. It is noted that not all chemical bonds form odd electron bonds upon losing one electron: Fig. S3 in the Supporting Information demonstrates that one-electron and three-electron bonds do not spontaneously form in nitrogen-nitrogen systems. Upon a single-electron removal from the N-N single bond, the SOMO is not localized between nitrogen atoms, nor does it exhibit σ- or π-orbital features observed in hydrocarbon cations (Fig. 2 (b)). Odd-electron bond formation requires precise geometric conditions—as demonstrated by the quintuple-bond candidate in Fig. S3(3), where electron density characterizes a N-N separation of 1.34 Å.

We show in Fig. 2(c) the Raman spectra of the three types of C–C cations with odd-electron bonds. Here the absence of imaginary frequencies validates the stability of these cations[43]. The ethane cation exhibits a lower frequency mode for its weaker one-electron σ-bond. In contrast, ethylene and ethyne cations display higher frequency peaks, in accord with their stronger π-bonds.

Table 1. The lengths and the energies of typical C–C bonds with a variety of shared electrons. Boldface in the second column represents the corresponding dissociated group.

Bond name	Typical formula	Atoms (C–C)	Bond length (Å)	Bond energy (kJ/mol)	Bond order	Bond strength (nN)
one-electron σ-bond (**1**$^{\cdot+}$)	$(C_{20}H_{13})\mathbf{C}\cdots C(C_{20}H_{13})$	$sp^3\cdots sp^3$	2.92[2]	86.4 (Derived)	0.216	0.66
one-electron σ-bond	$\mathbf{H_3C}\cdots CH_3^+$	$sp^3\cdots sp^3$	1.98	137.2	0.504	1.49
σ-bond	$\mathbf{H_3C}$–CH_3	sp^3–sp^3	1.53	407.8	1.157	6.59
σ-bond	$\mathbf{H_3C}$–CH=CH_2	sp^3–sp^2	1.50	426.3[44]	1.147	7.10
σ-bond	$\mathbf{H_3C}$–C_6H_5	sp^3–sp^2	1.51	426.8[44]	1.486	7.11
σ-bond	$\mathbf{H_3C}$–C≡CH	sp^3–sp	1.46	529.3[44]	1.172	7.90
σ-bond	$\mathbf{H_2C{=}HC}$–C≡CH	sp^2–sp	1.43	572.4[44]	1.188	8.51
σ-bond	$\mathbf{HC{\equiv}C}$–C≡CH	sp–sp	1.38	670.3[44]	1.262	11.41
delocalized π bond	graphene	sp^2–sp^2	1.42	601.9	1.333	9.10
delocalized π bond	C_6H_6	sp^2–sp^2	1.39[45]	509.5	1.658	—
three-electron bond	$\mathbf{H_2C}\cdot\cdot\cdot CH_2$	$sp^2\cdot\cdot\cdot sp^2$	1.42	696.8	1.668	10.89
σ+π bond	$\mathbf{H_2C}$=CH_2	sp^2=sp^2	1.32	792.4	2.148	14.65
five-electron bond	$\mathbf{HC}\dddot{=}$CH	$sp\dddot{=}sp$	1.26	828.1	2.643	21.81
σ+2π bond	$\mathbf{HC}$≡CH	sp≡sp	1.20	990.3	3.112	25.72

Several empirical relationships between bond length, bond energy, and vibrational force constants have long been established in chemical bonding theory. Pauling's work[1, 46] qualitatively correlated bond order with bond energy and inversely with bond length. Badger's rule[47] and Johnston's theorem[48] further linked bond length to force constants and bond energy. More recently, Kraka and coworkers[49] adopted bond critical point electron densities as a unified descriptor for bond strength. In contrast to these classical relationships, which focus on bond energy or small-deformation force constants, our work systematically investigates the rupture force—a direct measure of mechanical strength and the quantity accessible in single-molecule force spectroscopy experiments—across the full bond-order spectrum including odd-electron bonds. Moreover, we reveal element-dependent scaling coefficients and a negative intercept that together provide a complete picture of covalent bonding under tension.

The mechanical properties of C–C bonds from DFT calculations are shown in Fig. 3. The total potential energy as a function of bond distance for seven types of C–C bonds in Fig. 3(a) illustrates their distinction in both energy levels and in response to stretching (see Fig. 3(b) and Table 1 for an overview). Force versus bond separation curves, after the initial linear region, soon reach a force plateau, and then a softening region. The softening part can be well characterized in displacement-controlled loading but often leads to instantaneous bond breakage under force-controlled loading mode, in line with prior observations[50-52]. The combined representation in the inset in Fig. 3(b) is the detailed view of the one-electron bond (bond order = 0.504, $H_3C\cdots CH_3^+$). It highlights how the force-energy relationship evolves during bond separation: within the region of r_0 to r_m, increasing resistance to stretch occurs. After the force reaches its maximum (termed as the bond strength σ_m) at a critical length r_m[53], the chemical bond enters the softening regime where the attractive force diminishes with further separation. Among the diverse metrics for characterizing bond strength[53-55], the peak force serves as a convenient parameter quantifying the quasi-diatomic molecular systems. Although direct experimental measurement of an isolated C–C single bond rupture force remains challenging, extensive studies have validated the ability of DFT calculations to accurately predict bond rupture forces. For example, Grandbois et al. measured the rupture force of Si–C bonds using AFM (2.0 ± 0.3 nN) and found quantitative agreement with DFT calculations [50]. The emergence of imaginary frequencies in the phonon spectra of stretched lattice beyond

this point is a sign of lattice instability[56, 57]. In the softening region, the curves undergo abrupt changes at the point (marked off with '×' in Fig. 3(a-b)) when a π-bond breaks, consistent with the abrupt rupture observed at crack tips during crack propagation[58]. A greater number of shared electrons leads to shorter bonds (r_0) at equilibrium, and results in smaller critical length (r_m). Since bond order emerges as the decisive physical parameter governing the chemical bond contrast based on scanning probe microscopy[59, 60], We plot in Fig. 3(c) the changes in bond length, critical length and bond dissociation energy with different bond orders. All bond orders reported are Wiberg bond orders[61] computed from NBO analysis, which provides a consistent metric for comparing covalent interactions across diverse bonding environments, including odd-electron bonds and delocalized systems. A π-bond of graphene has a bond order of 1.333 and there is nil bond order for vdW interactions[62].

Bond stiffness k_b, defined as the slope of the force-distance curve at equilibrium, quantitatively describes a chemical bond's resistance to elastic deformation. The bond stiffness at the equilibrium configuration is highly correlated with bond strength, as shown in Fig. 3(d). While Pauling's valence bond theory qualitatively anticipated a correlation between bond order and bond energy, a quantitative verification spanning the full spectrum of bond orders—from the recently confirmed one-electron σ-bond to triple bonds—across multiple elements, using the experimentally relevant metric of bond strength (peak rupture force), remains unseen. The same linear scaling is also obtained at the MP2 and CCSD(T) levels (Fig. S10 in the supporting information), confirming its robustness. Excluding the vdW interaction, we see from Fig. 3(d) that the bond strength (σ_m) and bond order (n) exhibit a linear relation for C–C bonds that $\sigma_m = k \cdot n + \sigma_0$, where k = 8.9 nN/order, σ_0 = –2.8 nN, and the Pearson's correlation coefficient R = 0.995. The negative represents the contribution from non-covalent interactions (primarily Pauli repulsion) to the peak force at zero bond order. To the limit of n → 0, where no shared electrons exist between atoms, the interatomic interaction is dominated by repulsion and therefore a negative force. The bond order of the C···C interaction in cation $\mathbf{1}^{\cdot+}$ is 0.216 by performing NBO analysis, whereas that of an isolated σ-bond ($H_3C\cdots CH_3^+$) is 0.504. Their bond stiffnesses and bond strengths of cation $\mathbf{1}^{\cdot+}$ in Fig. 3(d) therefore fall at the lower end of the linear correlation. To assess the predictive capability of the empirical linear relationship $\sigma_m = 8.9n - 2.8$ (nN), we performed a blind test on a C–C bond system that is not included in the original fitting procedure. Specifically, we selected the C–C single bond in $H_3C–CH=CH_2$ (propene), which has a Wiberg bond order of 1.147 (as computed from NBO analysis at the M06-2X/6-311+G** level). The predicted bond strength is 7.4 nN. The calculated rupture force from the DFT force–distance curve is 7.1 nN (see Table 1). The discrepancy between the prediction and the calculation is only 4.2% which confirms the validity of the linear scaling.

C. General covalent systems

Building upon the established linear relationship between bond strength and bond order in C···C bonds, we further examine the generalizability of this correlation. We investigate 13 covalent systems across 7 elements (B, C, N, O, Si, P and S) , which possess substantial bonding strength and consequently superior material characteristics such as thermal conduction[63]. As shown in Fig. 4(a), all examined systems exhibit remarkable linearity between their bond strength and bond order, in agreement with the general form of $\sigma_m = k \cdot n + \sigma_0$. Resources and numerical data can be found in Table S1 in the supporting information. We note that for most element pairs, only a limited number of bond orders (typically 2–4) are available in stable quasi-diatomic systems. This is inherent to the simplified model design, which deliberately excludes environmental perturbations to isolate intrinsic bonding behavior. Nevertheless, the high

linearity observed for the C–C system and Si–Si system demonstrates its robustness. We note here that we have carried out systematic validation by adopting seven density functionals (M06-2X[64], PBE0[65], B3LYP[66], ωB97XD[67], TPSSh[68, 69], cam-B3LYP[70], and B2PLYP[71], and all independent calculations are detailed in Figs.S4-S9 of the Supporting Information), confirm the robustness of this linear relationship. For non-integer bond order predictions, we employed a strategy analogous to the C–C systems, and constructed quasi-diatomic molecular cations for comparative analysis. All examined systems display near-parallel regression lines with characteristic slopes ranging from 4 to 11 nN per bond order. We plot in Fig. 4(b) those element-dependent coefficients k. The specifics may originate from atomic radii, valence electron configuration, electronegativity and other features of elements. Notably, we observe that elements with smaller atomic radii and higher electronegativity (e.g., C, N, O) tend to exhibit larger slope of k, indicating a higher sensitivity of bond strength to bond order changes. In contrast, larger atomic radii and lower electronegative elements (e.g., Si, P, S) show smaller slopes. The linear scaling established here is validated for quasi-diatomic covalent bonds involving main-group elements in their ground electronic states. Its applicability to excited states, strongly correlated systems, or bonds under extreme strain beyond the peak force has not been tested and may require further investigation.

The linear correlation between bond strength and bond order, $\sigma_m = k \cdot n + \sigma_0$, established for 13 covalent systems, provides a quantitative foundation for tuning covalent bond strengths. Bond order engineering refers to the deliberate modulation of electron occupancy in bonding orbitals through chemical or physical means. Experimentally, many groups have demonstrated tunable bond order through redox reactions (e.g., oxidation of ethane to its cation reduces the C–C bond order from 1 to 0.5)[32, 34], by ligand effects that modify orbital overlap[72], or by external stimuli such as electric fields which have been shown to tune bond strength in single-molecule junctions[73]. The linear relationship derived here enables a quantitative prediction: for a desired bond strength, the required bond order can be directly estimated, and conversely, a change in bond order induced by molecular design is expected to yield a predictable change in bond strength. This framework thus bridges electronic structures to mechanical properties, offering a design guideline.

From an experimental standpoint, the linear relationship can be validated and exploited through several established techniques. Single-molecule force spectroscopy (SMFS) and atomic force microscopy (AFM) enable direct measurement of bond rupture forces, providing experimental benchmarks for the predicted bond strengths across different bond orders[50, 51]. Moreover, bond order modulation itself is experimentally accessible: redox chemistry offers reversible control over electron occupancy, while chemical synthesis enables systematic variation of bond orders through ligand design or incorporation of odd-electron bonds.

Following the guidance from Pauling that the shorter a chemical bond's length is, the greater its strength[46], a number of empirical formulae have been proposed relating bond length and bond strength. Recent work by Frenking and coworkers demonstrated that chemical bond strength can be effectively characterized at the equilibrium configuration[74]. To systematically compare the energetics of covalent bonds with conventional bond types (covalent, ionic, metallic, hydrogen, and vdW), we employ the bond dissociation energy and the bond length as the metrics (data involved with bond length from[21], and those of energy from[44], see Table S2 in the Supporting Information). Representative bond lengths (r_0) and bond energy (E_{BD}) for a great number of bond types are shown in Fig. 5. While we see the rough tradeoff of bond energy and bond length in a wide range of quasi-diatomic systems, the C–C bonds (black solid stars) based on our calculations demonstrates more clearly the linear correlation for the entire covalent spectrum from one-electron σ-bond at the lower boundary to the ultra-strong triple bond (σ+2π). We further demonstrate its validity in the inset based on our calculations for other covalent atomic pairs of distinct

bond orders. Here the energy level of one-electron σ-bonds sits at the lower bound of their respective covalent family.

In this study, we have successfully elucidated a unified mechanical framework for covalent bonds through first-principles investigations. The anomalous one-electron C···C σ-bond in cation $\mathbf{1}^{\cdot+}$, which owes a maximum bond strength of 3.00 nN, delineates the lower bound of covalent interactions. A linear correlation between bond strength and bond order across carbon covalence is revealed to be in the form $\sigma_m = k \cdot n + \sigma_0$, where k = 8.9 nN/order and σ_0 = –2.8 nN. Notably, this relationship transcends elemental specificity and is seen in 13 types of covalent interactions exhibiting multiple bond orders. We further observe that bond dissociation energy–bond length inverse correlation is also suitable for covalent with different bond orders, along with traditional covalent, ionic, metallic bonding and weak interaction regimes such as hydrogen bonding and vdW interactions[75, 76]. Although notable exceptions exist where stronger bonds aren't necessarily shorter[77], it is noted that the strength-bonder order correlation revealed here strictly applies to one specific type of bonds. Since tuning bond strengths by the placement of electron-withdrawing or –donating groups on a molecule is a promising routine of making new materials[73, 78, 79], we expect these insights may further supply guidance to the development of advanced materials of variable strengths through bond order modulation.

Methods

We adopt density functional theory (DFT) calculations analyzing the molecular structures, mechanical and electronic properties of those quasi-diatomic bonds. Unless stated otherwise, all DFT calculations are performed using Gaussian 16 package[80], which employs the M06-2X functional[64] with the 6-311+G** basis set[81, 82]. Such a combination is well-suited for describing the bonding and electronic properties of those covalent systems. Geometry optimization and frequency calculations are carried out to determine the equilibrium state of the molecules in question.

Bond order analysis

All bond orders reported in this work are Wiberg bond orders, which are defined within the natural bond orbital (NBO) framework as:

$$W_{AB} = \sum_{\mu \in A} \sum_{\nu \in B} (P_{\mu\nu})^2 \tag{1}$$

where $P_{\mu\nu}$ is the density matrix element between atomic orbitals μ and ν. The Wiberg bond order index provides a measure of the net covalent bonding interaction between two atoms and is well-defined for both closed-shell and open-shell systems, including both odd-electron bonds and delocalized structures.

Periodic systems calculations

For periodic systems such as graphene and graphite, we employed the Vienna Ab Initio Simulation Package (VASP) to perform DFT calculations[83]. In these calculations, the Perdew-Burke-Ernzerhof (PBE) functional[65, 84] is used to describe the exchange-correlation interactions, and the plane-wave basis set with a cutoff energy of 520 eV is adopted. DFT-D3 correction is used to account for the van der Waals (vdW) effect[85]. The Brillouin zone is sampled using a Monkhorst-Pack grid[86]. We use GaussView software[87] for molecular visualization, vibrational mode and Raman spectra analysis.

Visualization and analysis tools

The analysis of the singly-occupied molecular orbital (SOMO) which provides insights on the electronic structure of the one-electron bond is performed using Multiwfn[24]. We visualize the SOMO by using the Visual Molecular Dynamics (VMD) software[88].

Supporting Information.

Details of one-electron σ-bond of $\mathbf{1}^{\cdot+}$, cross-validation on C–C one-electron σ-bond, dataset of bond information and Systematic validation of linear bond strength and bond orders.

Data availability

The datasets include energy versus length trajectory by Gaussian for the 13 covalent systems and $\mathbf{1}^{\cdot+}$ and Raman spectra of the three types of C–C cations. They are available at https://github.com/zs-ustc/Linear-bond-strength-bond-order-relationship-in-covalent-interactions.

References

[1] Pauling, L., The nature of the chemical bond. II. The one-electron bond and the three-electron bond. *J. Am. Chem. Soc.* **53**, 9 (1931).

[2] Shimajiri, T., Kawaguchi, S., Suzuki, T. & Ishigaki, Y., Direct evidence for a carbon–carbon one-electron σ-bond. *Nature* (2024).

[3] Zum Bezolproblem, Q. B. & zum Problem, Q. B., Quantentheoretische beiträge zum benzolproblem. *Z. Phys. Chem.* **70** (1931).

[4] Coulson, C., Valency: Classical and Modern. *Nature* **154** (1944).

[5] Pauling, L., The nature of the chemical bond—1992. *J. Chem. Educ.* **69**, 7 (1992).

[6] Zheng, X., et al., Twist-assisted intrinsic toughening in two-dimensional transition metal dichalcogenides. *Nat. Mater.* (2025).

[7] Jin, R., Yuan, X. & Gao, E., Atomic stiffness for bulk modulus prediction and high-throughput screening of ultraincompressible crystals. *Nat. Commun.* **14**, 1 (2023).

[8] Inagaki, M. & Kang, F., Materials science and engineering of carbon: fundamentals (Butterworth-Heinemann, 2014).

[9] Ferrari, A. C., Determination of bonding in diamond-like carbon by Raman spectroscopy. *Diamond Relat. Mater.* **11**, 3-6 (2002).

[10] Wallace, P. R., The band theory of graphite. *Phys. Rev.* **71**, 9 (1947).

[11] Pauling, L. & Yost, D. M., The additivity of the energies of normal covalent bonds. *Proc. Natl. Acad. Sci.* **18**, 6 (1932).

[12] Hirshfeld, F., Electron density distributions in molecules. *Crystallogr. Rev.* **2**, 4 (1991).

[13] March, N. H., Parr, R. G. & Mucci, J. F., The kinetic energy change on covalent bond formation. *Proc. Natl. Acad. Sci.* **78**, 10 (1981).

[14] Dudko, O. K., Hummer, G. & Szabo, A., Theory, analysis, and interpretation of single-molecule force spectroscopy experiments. *Proc. Natl. Acad. Sci.* **105**, 41 (2008).

[15] Ortiz, J., Toward an exact one-electron picture of chemical bonding. *Adv. Quantum Chem.* **35** (1999).
[16] Feinberg, M. & Ruedenberg, K., Heteropolar One‐Electron Bond. *J. Chem. Phys.* **55**, 12 (1971).
[17] Hübner, A., et al., Confirmed by X‐ray Crystallography: The B· B One‐Electron σ Bond. *Angew. Chem.* **126**, 19 (2014).
[18] Brockway, L. O., The three-electron bond in chlorine dioxide. *Proc. Natl. Acad. Sci.* **19**, 3 (1933).
[19] Mayer, I., Atomic orbitals from molecular wave functions: The effective minimal basis. *J. Phys. Chem.* **100**, 15 (1996).
[20] Grimvall, G., Thermophysical properties of materials (Elsevier, 1999).
[21] Johnson, R. D., NIST computational chemistry comparison and benchmark database. (2022).
[22] Weinhold, F. & Landis, C. R., Valency and bonding: a natural bond orbital donor-acceptor perspective (Cambridge University Press, 2005).
[23] Sauers, R. R., A natural bond orbital analysis of carbanions. *Computational and Theoretical Chemistry* **999** (2012).
[24] Lu, T. & Chen, F., Multiwfn: A multifunctional wavefunction analyzer. *J. Comput. Chem.* **33**, 5 (2012).
[25] Bader, R. F., Atoms in molecules. *Acc. Chem. Res.* **18**, 1 (1985).
[26] Cremer, D. & Kraka, E., A description of the chemical bond in terms of local properties of electron density and energy. *Croat. Chem. Acta* **57**, 6 (1984).
[27] Laidig, K. E. & Bader, R. F., Properties of atoms in molecules: Atomic polarizabilities. *J. Chem. Phys.* **93**, 10 (1990).
[28] Goulielmakis, E., et al., Real-time observation of valence electron motion. *Nature* **466**, 7307 (2010).
[29] Levine, I. N., Busch, D. H. & Shull, H., Quantum chemistry 6 (Upper Saddle River, NJ: Pearson Prentice Hall, 2009).
[30] Beyer, M. K. & Clausen-Schaumann, H., Mechanochemistry: the mechanical activation of covalent bonds. *Chem. Rev.* **105**, 8 (2005).
[31] Huang, M.-B. & Lunell, S., Equilibrium structure and hyprfine parameters of the ethane cation. *Chem. Phys.* **147**, 1 (1990).
[32] Lee, K. L. K., Rabidoux, S. M. & Stanton, J. F., Cation states of ethane: HEAT calculations and vibronic simulations of the photoelectron spectrum of ethane. *J. Phys. Chem. A* **120**, 38 (2016).
[33] Lunell, S. & Huang, M.-B., Theoretical confirmation of the esr spectrum of the ethane cation. *J. Chem. Soc., Chem. Commun.*, 15 (1989).
[34] Toriyama, K., Nunome, K. & Iwasaki, M., Structures and reactions of radical cations of some prototype alkanes in low temperature solids as studied by ESR spectroscopy. *J. Chem. Phys.* **77**, 12 (1982).
[35] Zuilhof, H., Dinnocenzo, J. P., Reddy, C. & Shaik, S., Comparative study of ethane and propane cation radicals by B3LYP density functional and high-level ab initio methods. *J. Phys. Chem.* **100**, 39 (1996).
[36] Kim, M. H., Leskiw, B. D. & Suits, A. G., Vibrationally mediated photodissociation of ethylene cation by reflectron multimass velocity map imaging. *J. Phys. Chem. A* **109**, 35 (2005).
[37] Ludwig, A., et al., Ultrafast relaxation dynamics of the ethylene cation c2h4+. *J. Phys. Chem. Lett.* **7**, 10 (2016).
[38] Joalland, B., Mori, T., Martínez, T. J. & Suits, A. G., Photochemical dynamics of ethylene cation c2h4+. *J. Phys. Chem. Lett.* **5**, 8 (2014).

[39] Lorquet, J., Sannen, C. & Raseev, G., Dissociation of the ethylene cation: mechanism of energy randomization. *J. Am. Chem. Soc.* **102**, 27 (1980).
[40] Richardson, V., et al., Reactivity of the Ethenium Cation (C2H5+) with Ethyne (C2H2): A Combined Experimental and Theoretical Study. *Molecules* **29**, 4 (2024).
[41] Thissen, R., et al., Dissociations of the ethyne dication C2H2+ 2. *J. Chem. Phys.* **99**, 9 (1993).
[42] Kohn, W. & Sham, L. J., Self-consistent equations including exchange and correlation effects. *Phys. Rev.* **140**, 4A (1965).
[43] Meier, R. J., Calculating the vibrational spectra of molecules: An introduction for experimentalists with contemporary examples. *Vib. Spectrosc* **43**, 1 (2007).
[44] Luo, Y.-R., Comprehensive handbook of chemical bond energies (CRC press, 2007).
[45] Bacon, G., Curry, N. T. & Wilson, S., A crystallographic study of solid benzene by neutron diffraction. *Proc. R. Soc. London, Ser. A* **279**, 1376 (1964).
[46] Pauling, L., The nature of the chemical bond and the structure of molecules and crystals: an introduction to modern structural chemistry 18 (Cornell university press, 1960).
[47] Badger, R. M., A relation between internuclear distances and bond force constants. *The Journal of Chemical Physics* **2**, 3 (1934).
[48] Johnston, H. S., Continuity of bond force constants between normal molecules and Lennard-Jones pairs. *J. Am. Chem. Soc.* **86**, 8 (1964).
[49] Delgado, A. A. A., et al., Exceptionally Long Covalent CC Bonds—A Local Vibrational Mode Study. *Molecules* **26**, 4 (2021).
[50] Grandbois, M., et al., How strong is a covalent bond? *Science* **283**, 5408 (1999).
[51] Frei, M., et al., Mechanics and chemistry: single molecule bond rupture forces correlate with molecular backbone structure. *Nano Lett.* **11**, 4 (2011).
[52] Karácsony, O. & Akhremitchev, B. B., On the detection of single bond ruptures in dynamic force spectroscopy by AFM. *Langmuir* **27**, 18 (2011).
[53] Tolladay, M., Scarpa, F. & Allan, N. L., Interatomic forces breaking carbon-carbon bonds. *Carbon* **175** (2021).
[54] Esser, M., Esser, A. A., Proserpio, D. M. & Dronskowski, R., Bonding analyses of unconventional carbon allotropes. *Carbon* **121** (2017).
[55] Görne, A. L. & Dronskowski, R., Covalent bonding versus total energy: On the attainability of certain predicted low-energy carbon allotropes. *Carbon* **148** (2019).
[56] Liu, F., Ming, P. & Li, J., Ab initio calculation of ideal strength and phonon instability of graphene under tension. *Phys. Rev. B* **76**, 6 (2007).
[57] Wang, B., et al., Stable planar single-layer hexagonal silicene under tensile strain and its anomalous Poisson's ratio. *Appl. Phys. Lett.* **104**, 8 (2014).
[58] Jiang, S., et al., Unified fracture criterion for brittle 2D materials. *npj Comput. Mater.* **12**, 1 (2026).
[59] Ellner, M., Pou, P. & Pérez, R., Molecular identification, bond order discrimination, and apparent intermolecular features in atomic force microscopy studied with a charge density based method. *ACS Nano* **13**, 1 (2019).
[60] Wang, D., et al., Recent progress of imaging chemical bonds by scanning probe microscopy: a review. *ACS Nano* **18**, 45 (2024).
[61] Wiberg, K. B., Application of the pople-santry-segal CNDO method to the cyclopropylcarbinyl and cyclobutyl cation and to bicyclobutane. *Tetrahcdron* **24**, 3 (1968).
[62] Castro Neto, A. H., et al., The electronic properties of graphene. *Rev. Mod. Phys.* **81**, 1 (2009).
[63] Chen, J., et al., Accelerating discovery of next-generation power electronics materials via high-throughput ab initio screening. *npj Comput. Mater.* **11**, 1 (2025).

[64] Zhao, Y. & Truhlar, D. G., The M06 suite of density functionals for main group thermochemistry, thermochemical kinetics, noncovalent interactions, excited states, and transition elements: two new functionals and systematic testing of four M06-class functionals and 12 other functionals. *Theor. Chem. Acc.* **120** (2008).
[65] Perdew, J. P., Burke, K. & Ernzerhof, M., Generalized gradient approximation made simple. *Phys. Rev. Lett.* **77**, 18 (1996).
[66] Stephens, P. J., Devlin, F. J., Chabalowski, C. F. & Frisch, M. J., Ab initio calculation of vibrational absorption and circular dichroism spectra using density functional force fields. *J. Phys. Chem.* **98**, 45 (1994).
[67] Chai, J.-D. & Head-Gordon, M., Long-range corrected hybrid density functionals with damped atom–atom dispersion corrections. *Phys. Chem. Chem. Phys.* **10**, 44 (2008).
[68] Staroverov, V. N., Scuseria, G. E., Tao, J. & Perdew, J. P., Comparative assessment of a new nonempirical density functional: Molecules and hydrogen-bonded complexes. *J. Chem. Phys.* **119**, 23 (2003).
[69] Tao, J., Perdew, J. P., Staroverov, V. N. & Scuseria, G. E., Climbing the density functional ladder: Nonempirical meta–generalized gradient approximation designed for molecules and solids. *Phys. Rev. Lett.* **91**, 14 (2003).
[70] Yanai, T., Tew, D. P. & Handy, N. C., A new hybrid exchange–correlation functional using the Coulomb-attenuating method (CAM-B3LYP). *Chem. Phys. Lett.* **393**, 1-3 (2004).
[71] Grimme, S., Ehrlich, S. & Goerigk, L., Effect of the damping function in dispersion corrected density functional theory. *J. Comput. Chem.* **32**, 7 (2011).
[72] Tolman, C. A., Steric effects of phosphorus ligands in organometallic chemistry and homogeneous catalysis. *Chem. Rev.* **77**, 3 (1977).
[73] Omidian, M., et al., Electric-field control of a single-atom polar bond. *Phys. Rev. Lett.* **126**, 21 (2021).
[74] Zhao, L., Zhi, M. & Frenking, G., The strength of a chemical bond. *Int. J. Quantum Chem.* **122**, 8 (2022).
[75] Kaupp, M., Danovich, D. & Shaik, S., Chemistry is about energy and its changes: A critique of bond-length/bond-strength correlations. *Coord. Chem. Rev.* **344** (2017).
[76] Alkorta, I., Rozas, I. & Elguero, J., Bond length–electron density relationships: from covalent bonds to hydrogen bond interactions. *Struct. Chem.* **9** (1998).
[77] Kaupp, M., Metz, B. & Stoll, H., Breakdown of Bond Length ‐ Bond Strength Correlation: A Case Study. *Angew. Chem. Int. Ed.* **39**, 24 (2000).
[78] Ball, P., Tuning a bond. *Nat. Mater.* **20**, 7 (2021).
[79] You, S., et al., Identifying Carbon–Carbon Triple Bonds from Double Bonds via Single-Molecule Conductance. *ACS Nano* **19**, 4 (2025).
[80] Frisch, M. J., et al., Gaussian 16 Revision B.012016).
[81] McLean, A. & Chandler, G., Contracted Gaussian basis sets for molecular calculations. I. Second row atoms, Z= 11–18. *J. Chem. Phys.* **72**, 10 (1980).
[82] Krishnan, R., Binkley, J. S., Seeger, R. & Pople, J. A., Self ‐ consistent molecular orbital methods. XX. A basis set for correlated wave functions. *J. Chem. Phys.* **72**, 1 (1980).
[83] Kresse, G. & Furthmüller, J., Efficiency of ab-initio total energy calculations for metals and semiconductors using a plane-wave basis set. *Comput. Mater. Sci.* **6**, 1 (1996).
[84] Blöchl, P. E., Projector augmented-wave method. *Phys. Rev. B* **50**, 24 (1994).
[85] Grimme, S., Antony, J., Ehrlich, S. & Krieg, H., A consistent and accurate ab initio parametrization of density functional dispersion correction (DFT-D) for the 94 elements H-Pu. *J. Chem. Phys.* **132**, 15 (2010).

[86] Monkhorst, H. J. & Pack, J. D., Special points for Brillouin-zone integrations. *Phys. Rev. B* **13**, 12 (1976).
[87] Dennington, R., Keith, T. A. & Millam, J. M., GaussView, version 6.0.16 (Semichem Inc., Shawnee Mission, KS, 2016).
[88] Humphrey, W., Dalke, A. & Schulten, K., VMD: visual molecular dynamics. *J. Mol. Graphics* **14**, 1 (1996).

Figure Legends

Figure. 1. Deformation behavior of a one-electron σ-bond as a function of separation between the C···C bond in cation $\mathbf{1}^{\cdot+}$. (a) Molecular structure of $\mathbf{1}^{\cdot+}$ viewed from different perspectives. Here θ denotes the dihedral angle between the van der Waals (vdW) planes of proximal aryl fragments (determined by three-atom coordinates in each central carbon ring). (b) The relative energy (solid black) and force (solid red) versus C···C bond distance of the molecular shown in (a). The relative energy is the variance in total potential energy from its equilibrium configuration. Dashed lines are the corresponding terms of the isolated σ-bond in $H_3C\cdots CH_3^+$ molecule. (c) The interaction energy between the C···C bonded C atoms in cation $\mathbf{1}^{\cdot+}$ from calculations using energy decomposition analysis (EDA) method (solid black) and its derived force (solid red). (d) Snapshots (following the sequence keyed on the solid black curve in (b)) of the singly-occupied molecular orbitals (SOMOs), indicating the variation in electronic distribution while straining the C···C bond.

Figure 2. C–C interactions through odd-electron bonds. (a) Redox interconversion among ethane, ethylene, and ethyne cations. (b) Kohn-Sham orbitals of the SOMO for each cation. (c) Simulated Raman spectra of the three types of C–C cations.

Figure 3. Properties of C–C bonds with various shared electrons. (a) Bond potential energy versus bond distance curves for C–C bonds (with a zero-energy point related to the dissociated state), where '×' marks off the breakage of π-bond beyond which the energy curve undergoes an abrupt drop. (b) Force exerted on the bond as a function of bond distance, with peak load labelled with circles. Detailed view of the one-electron bond (bond order = 0.504, $H_3C\cdots CH_3^+$) showing combined force-energy relationship, where the blue curve (left axis) represents the potential energy and the red curve (right axis) for the force. (c) Bond length (r_0), critical length (r_m) and bond dissociation energy (E_{BD}) against bond order. (d) Bond stiffness (k_b, slope at the nil force point in 'b') compared to bond strength (σ_m).

Figure 4. Universal linear correlation between bond strength and bond order. (a) Calculated bond strength vs. bond order for various covalent systems with linear regression analysis. (b) Corresponding Pearson correlation coefficients R and linear slopes k for each type of covalent systems at UM06-2X/6-311+G** level.

Figure 5. Bond dissociation energy versus length over a wide range of quasi-diatomic systems demonstrating a bond energy-bond length tradeoff. Here C–C bonds with exceptional high potential energy from our study are highlighted with black stars. In the inset, we show the log-log plot of bond dissociation energy versus length of the 13 covalent systems reported here.

Author Contributions

Y.-J.W., Q.P. and Y.N. designed research; S.Z. and Y.-J.W. performed calculation research; S.Z, Y.-J.W., and Q.P. analyzed data; S.Z. and Y.-J.W. wrote the paper; Y.-J.W., Q.P., and Y.N. polished the language and revised the paper. All the authors contributed to the idea and reviewed the manuscript.

Acknowledgements

Y. Wei acknowledges support from the National Natural Science Foundation of China (NSFC) Basic Science Center for "Multiscale Problems in Nonlinear Mechanics", China (No. 12588201). The funder (NSFC) had no role in study design, data collection and analysis, decision to publish, or preparation of the manuscript.

Competing interests

The authors declare no competing financial or non-financial interest.

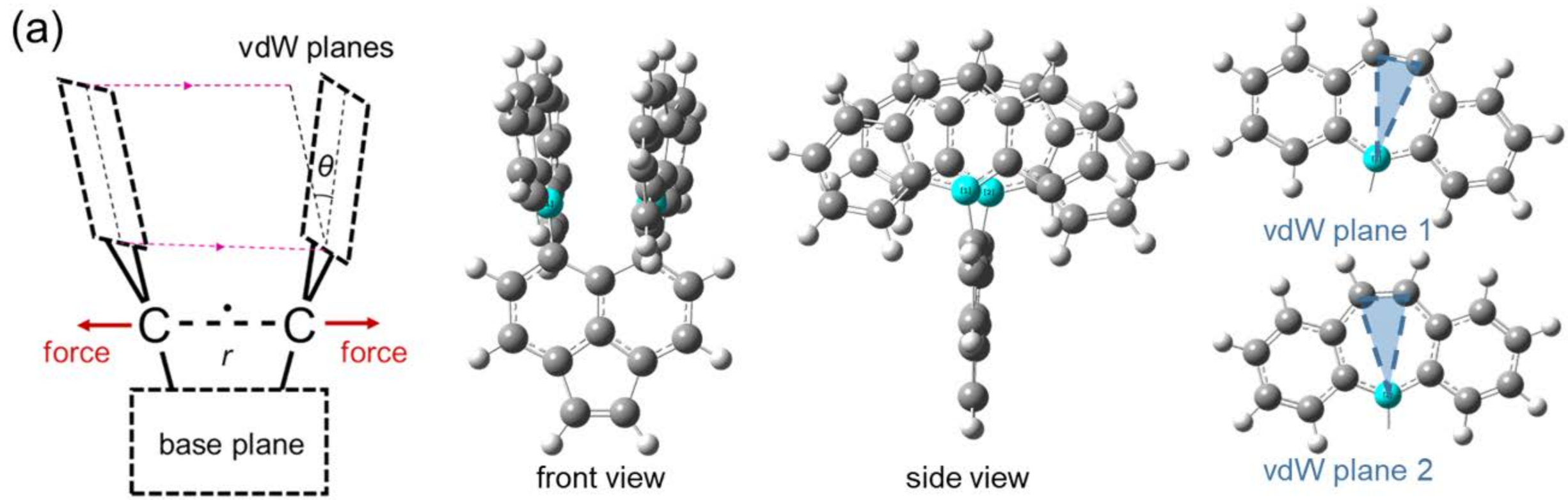
(a)
vdW planes
θ
C
C
force
force
r
base plane
front view
side view
vdW plane 1
vdW plane 2
(b)
Isolated σ-bond (energy)
Isolated σ-bond (force)
1·+ (energy)
1·+ (force)
Relative energy (eV)
Force (nN)
r − r0 (Å)
r0 = 2.853 (Å)
1
2
3
4
5
(c)
Isolated σ-bond (energy)
Isolated σ-bond (force)
σ-bond in 1·+ (energy)
σ-bond in 1·+ (force)
Relative energy (eV)
Force (nN)
r − r0 (Å)
r0 = 2.853 (Å)
(d)
1
2
3
4
5
r − r0 = −0.86 Å
θ = 20°
r − r0 = −0.60 Å
θ = 17°
r − r0 = 0 Å
θ = 9°
r − r0 = 0.26 Å
θ = 6°
r − r0 = 0.77 Å
θ = 30°

(a)

$H_3C—CH_3$ $H_2C=CH_2$ $HC\equiv CH$

+1e⁻ −1e⁻ +1e⁻ −1e⁻ +1e⁻ −1e⁻

$H_3C\cdots CH_3^+$ $H_2C\cdots CH_2^+$ $HC\equiv CH^+$

(b)

$H_3C\cdots CH_3^+$ $H_2C\cdots CH_2^+$ $HC\equiv CH^+$

(c)

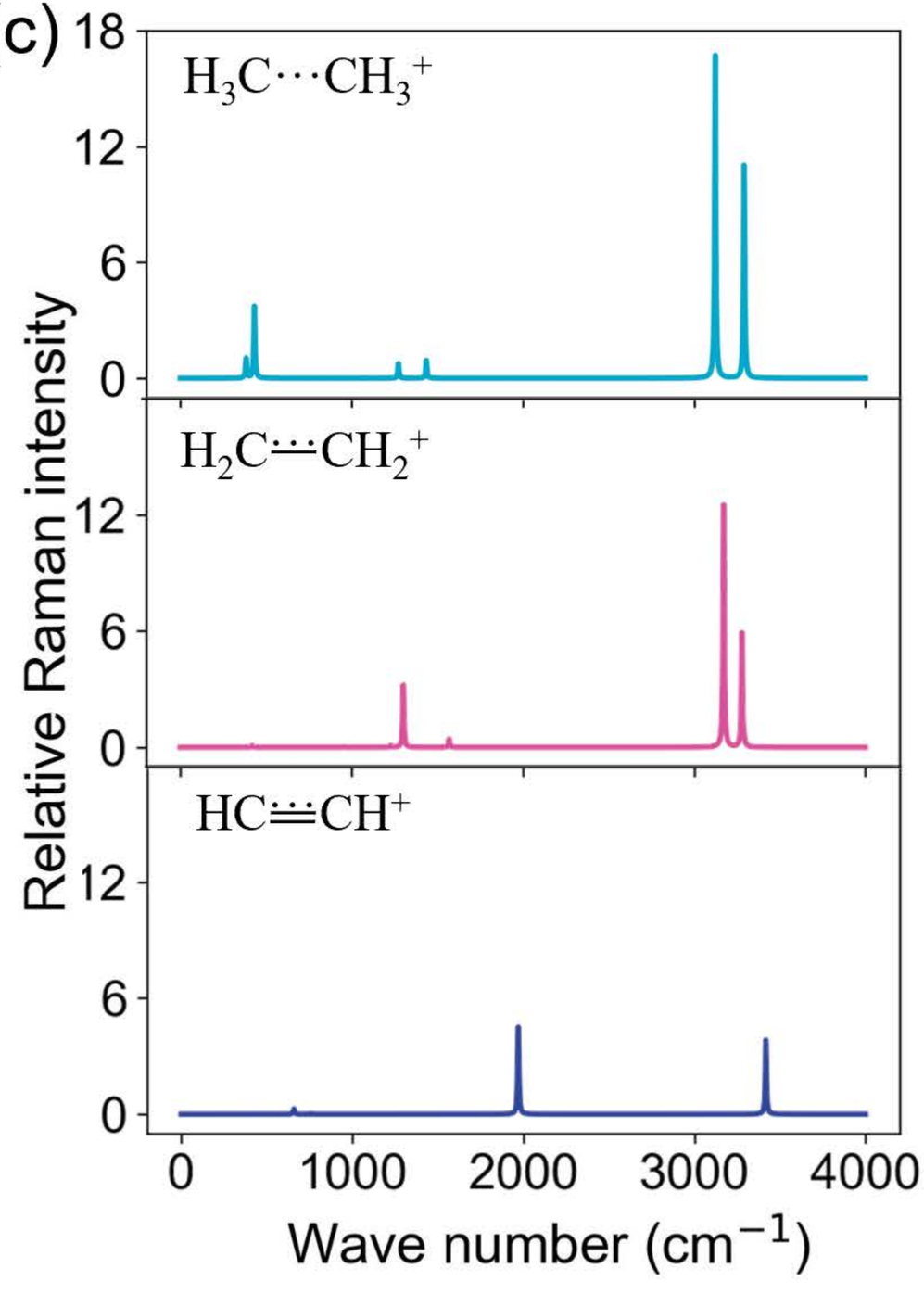

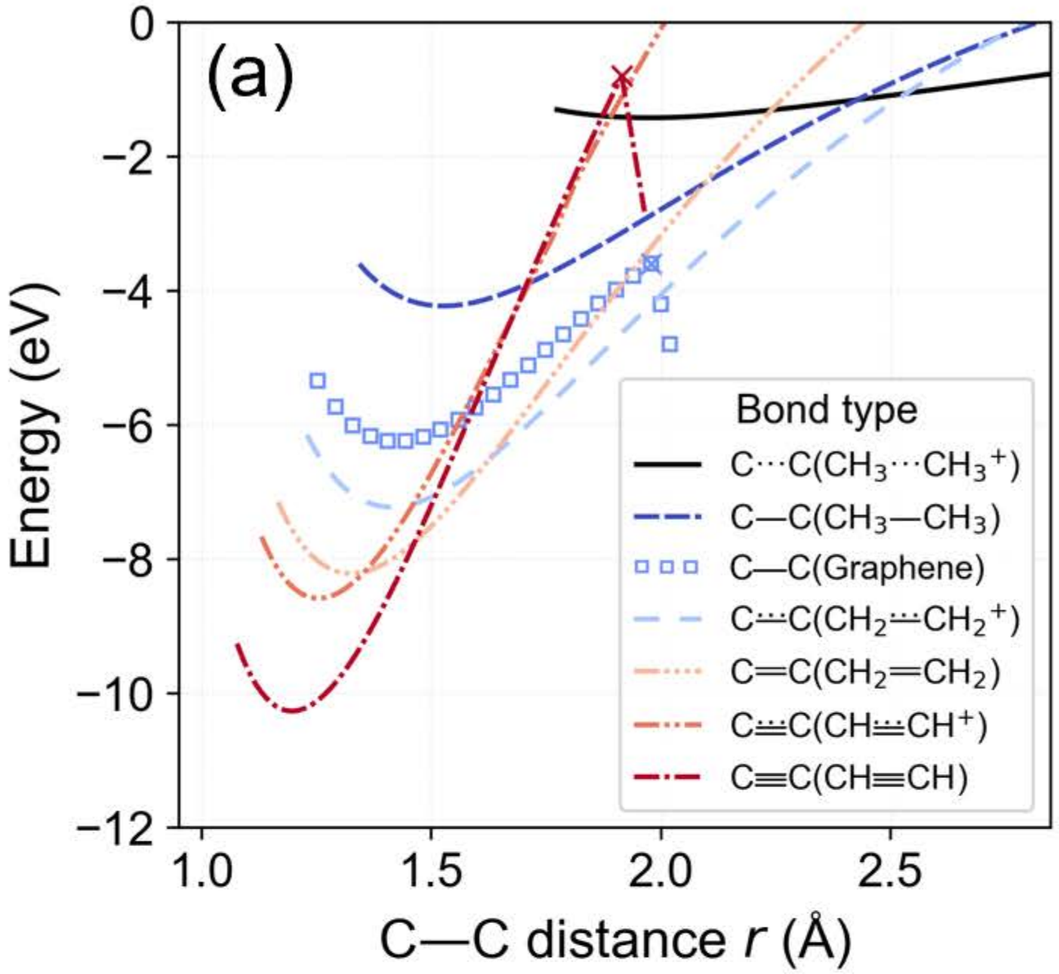
(a)
Energy (eV)
C—C distance r (Å)
Bond type
C···C(CH3···CH3+)
C—C(CH3—CH3)
C—C(Graphene)
C···C(CH2···CH2+)
C=C(CH2=CH2)
C···C(CH···CH+)
C≡C(CH≡CH)

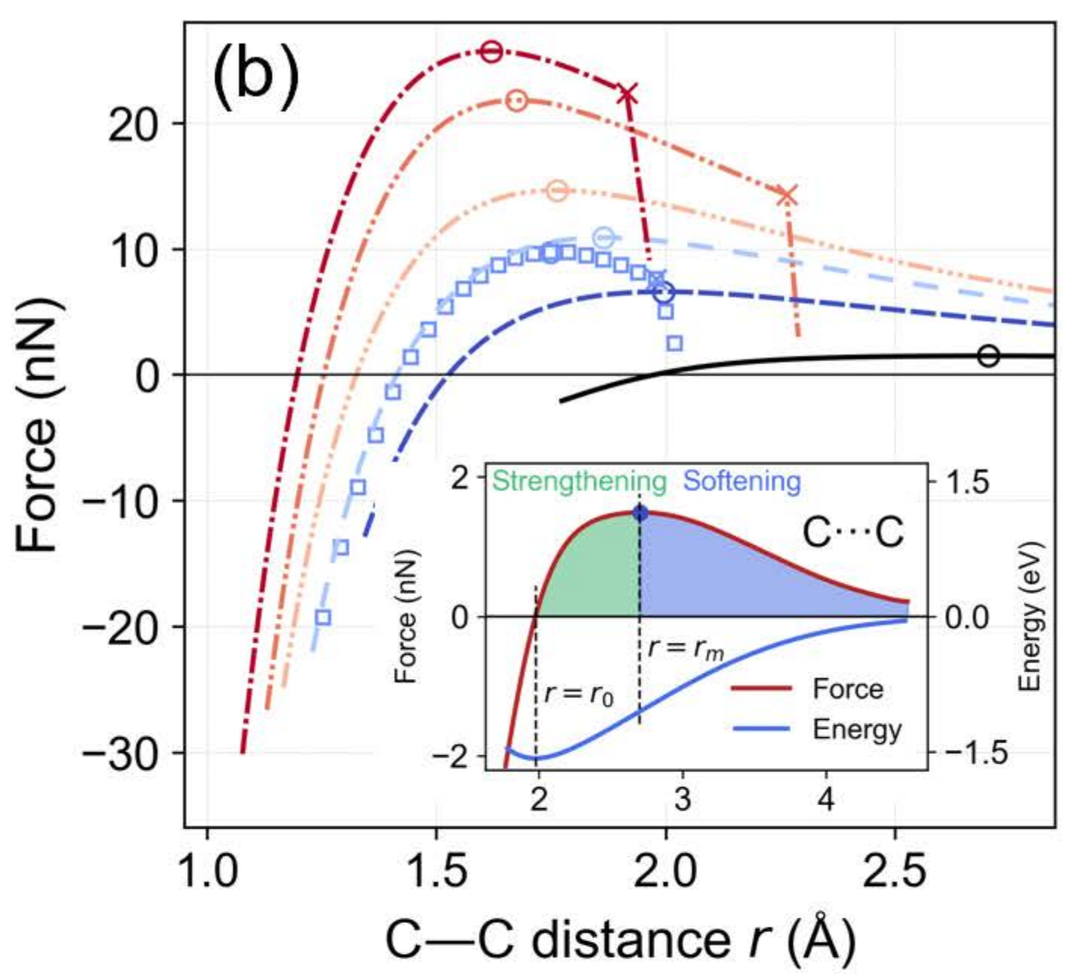
(b)
Force (nN)
C—C distance r (Å)
Strengthening
Softening
C···C
Force (nN)
Energy (eV)
r = r0
r = rm
Force
Energy

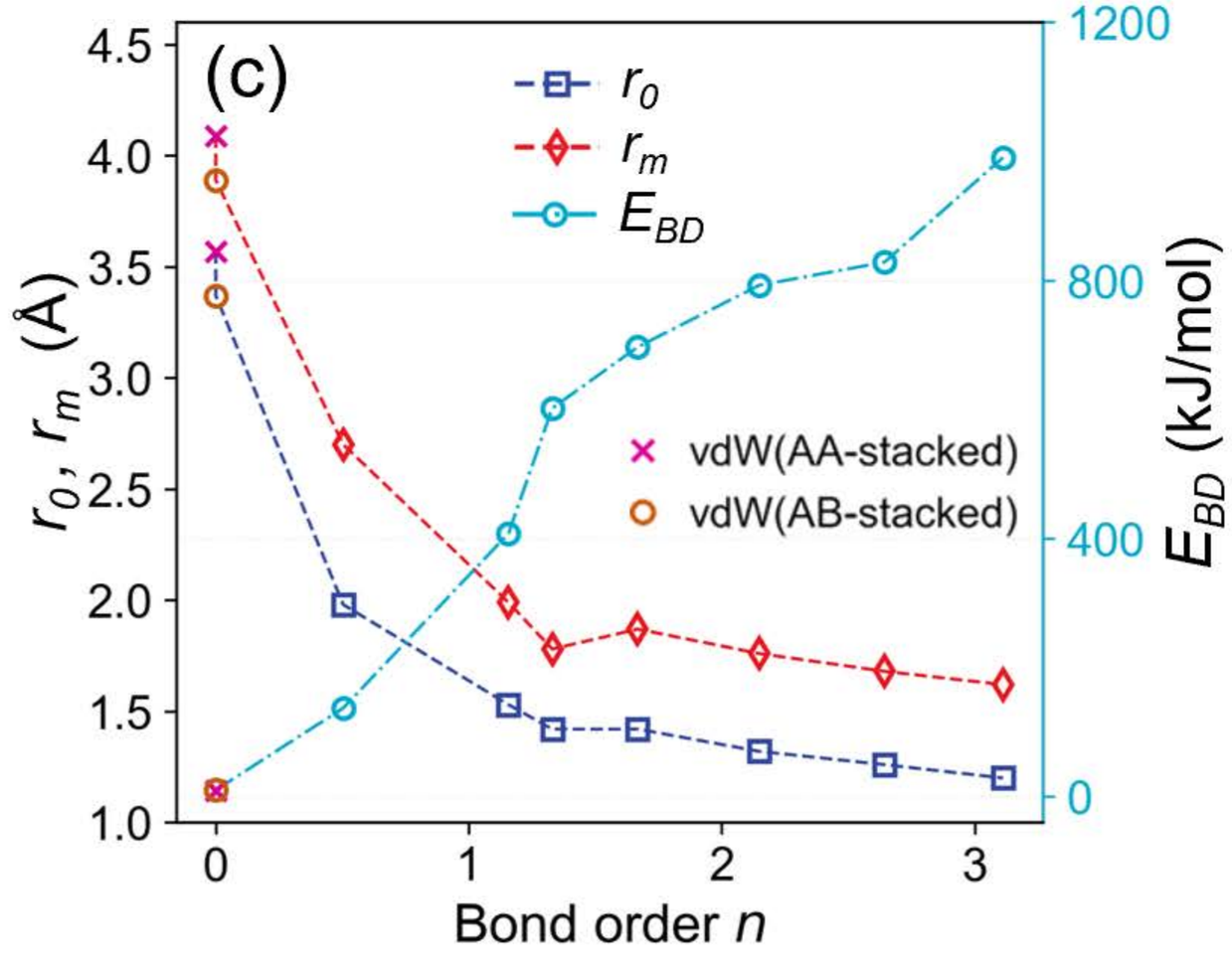
(c)
r0
rm
EBD
vdW(AA-stacked)
vdW(AB-stacked)
r0, rm (Å)
EBD (kJ/mol)
Bond order n

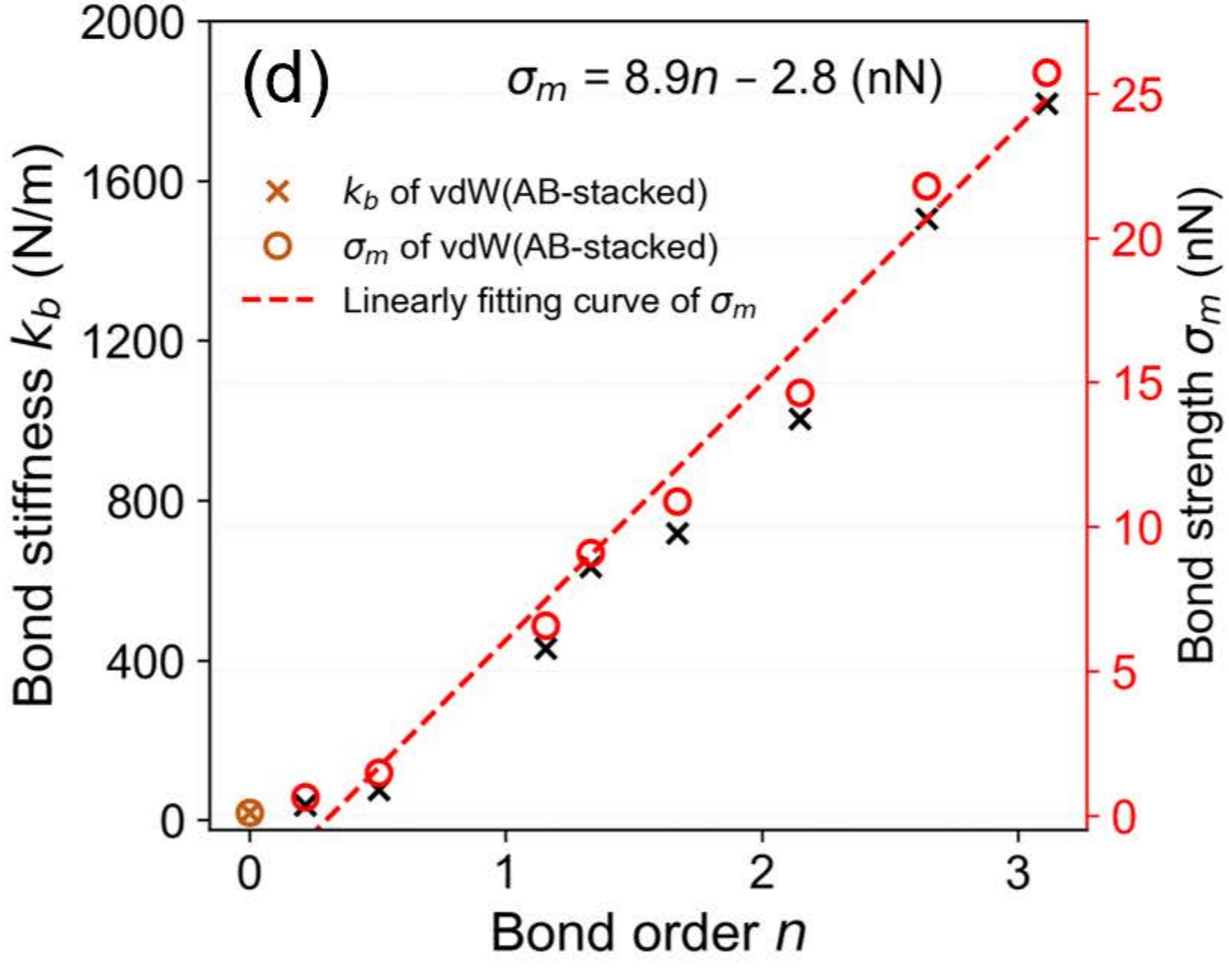
(d)
σm = 8.9n − 2.8 (nN)
kb of vdW(AB-stacked)
σm of vdW(AB-stacked)
Linearly fitting curve of σm
Bond stiffness kb (N/m)
Bond strength σm (nN)
Bond order n

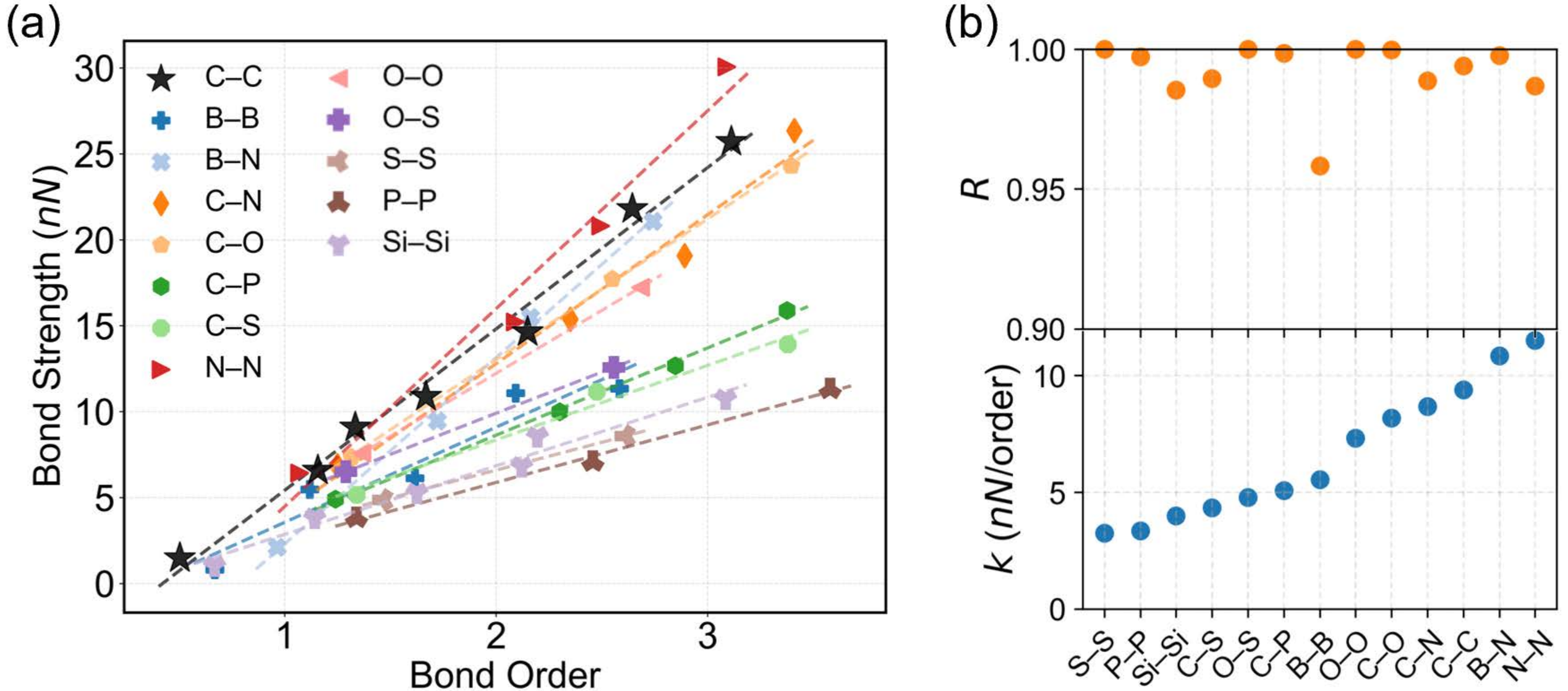
(a)
Bond Strength (nN)
Bond Order
C–C
B–B
B–N
C–N
C–O
C–P
C–S
N–N
O–O
O–S
S–S
P–P
Si–Si
(b)
R
k (nN/order)
S–S
P–P
Si–Si
C–S
O–S
C–P
B–B
O–O
C–O
C–N
C–C
B–N
N–N

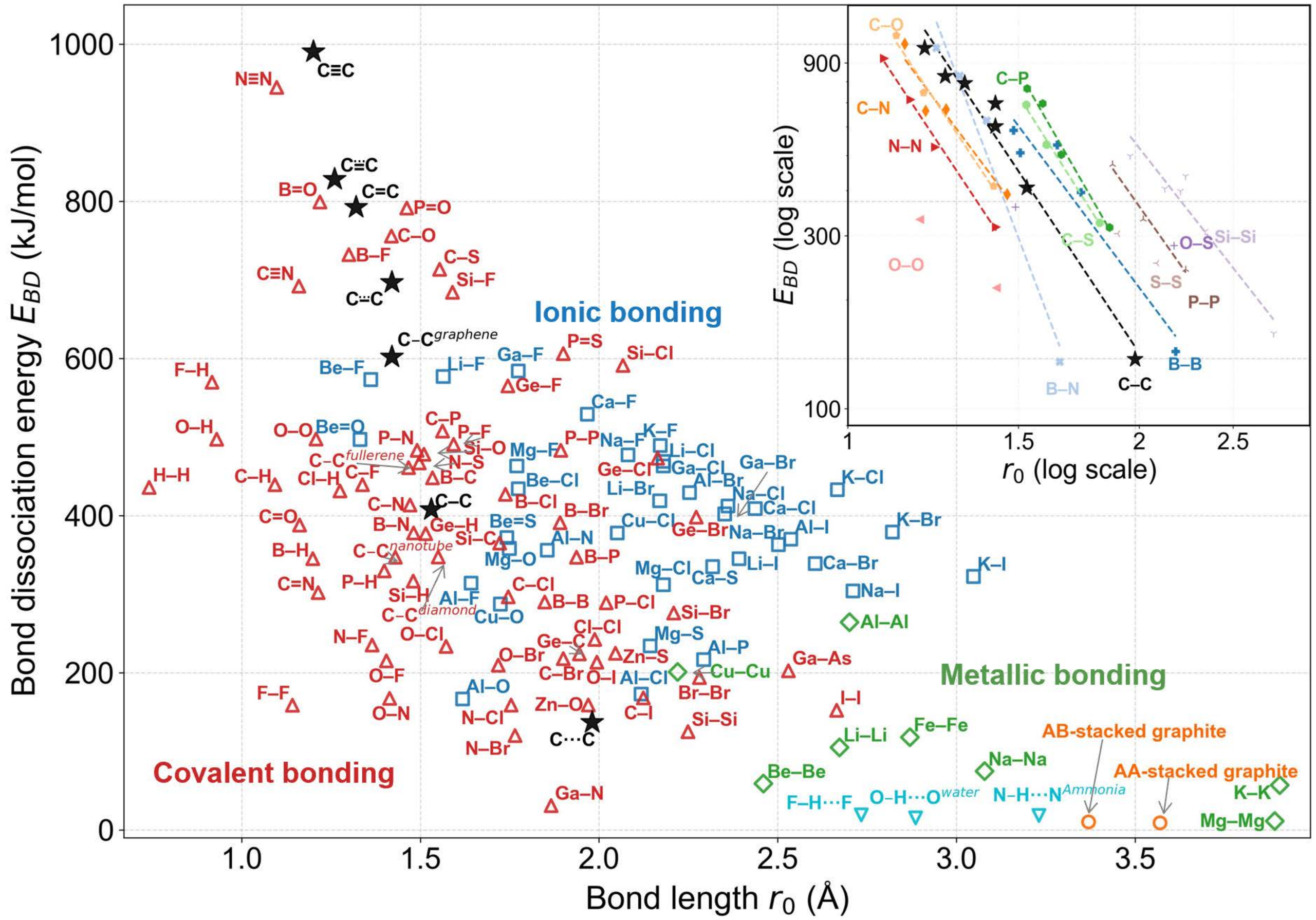
Bond dissociation energy E_{BD} (kJ/mol)
Bond length r_0 (Å)
E_{BD} (log scale)
r_0 (log scale)
Ionic bonding
Covalent bonding
Metallic bonding
C–O
C–N
N–N
O–O
C–P
C–S
S–S
P–P
O–S
Si–Si
B–B
B–N
C–C
C≡C
N≡N
C=C
B=O
ΔP=O
ΔC–O
ΔB–F
C–S
C≡N
Si–F
C···C
C–C graphene
P=S
Si–Cl
F–H
Be–F
Li–F
Ga–F
Ge–F
Ca–F
O–H
O–O
Be=O
C–P
P–F
P–N
Si–O
Mg–F
P–P
Na–F
K–F
Li–Cl
C–C fullerene
C–F
N–S
Ge–Cl
Ga–Cl
Ga–Br
H–H
C–H
Cl–H
B–C
Be–Cl
Li–Br
Al–Br
K–Cl
C–N
C–C
B–Cl
Na–Cl
Ca–Cl
C=O
B–Br
Cu–Cl
Be=S
Ge–Br
Na–Br
Al–I
K–Br
B–N
Ge–H
Si–C
Al–N
B–H
C–C nanotube
Mg–O
ΔB–P
Mg–Cl
Ca–S
Li–I
Ca–Br
K–I
C=N
P–H
Si–H
Al–F
C–Cl
Na–I
C–C diamond
Cu–O
ΔB–B
ΔP–Cl
Si–Br
Al–Al
Cl–Cl
N–F
O–Cl
Ge–C
Mg–S
O–Br
Zn–S
Al–P
Ga–As
O–F
C–Br
O–I
Al–Cl
Cu–Cu
F–F
Al–O
Br–Br
I–I
Zn–O
C–I
Si–Si
O–N
N–Cl
Li–Li
Fe–Fe
AB-stacked graphite
N–Br
Na–Na
Be–Be
AA-stacked graphite
Ga–N
F–H···F
O–H···O water
N–H···N Ammonia
K–K
Mg–Mg